Linear magnetoresistivity in the ternary AM_2B_2 and $A_3Rh_8B_6$ phases (A = Ca, Sr; M = Rh, Ir)

Hiroyuki Takeya*
National Institute for Materials Science,1-2-1 Sengen, Tsukuba, Ibaraki 305-0047, Japan and
JST, Transformative Research Project on Iron Pnictides (TRIP), Chiyoda, Tokyo 102-0075, Japan

Mohammed ElMassalami†
Instituto de Fisica, Universidade Federal do Rio de Janeiro, Caixa Postal 68528, 21945-970, Rio de Janeiro, Brazil
(Received 26 March 2011; revised manuscript received 3 June 2011; published 18 August 2011)

We studied the magnetoresistivity of the AM_2B_2 and $A_3Rh_8B_6$ (A = Ca, Sr; M = Rh, Ir) compounds within the ranges $1.8 \leqslant T \leqslant 300$ K and $0 \leqslant H \leqslant 50$ kOe. The zero-field resistivity $\rho_0(T)$ is metallic and follows closely the Bloch-Grüneisen description. A positive, nonsaturating, and dominantly linear-in-H magnetoresistivity was observed in all samples, including the ones with a superconducting ground state. Such $\Delta\rho_T(H)/\rho_T(0)$, reaching 1200% in favorable cases, was found to be much stronger for the AM_2B_2 compounds and to decrease with temperature as well as when Ca is replaced by Sr, or Rh is replaced by Ir. Finally, the general features of the observed magnetoresistivity will be discussed in terms of the Abrikosov model for the linear magnetoresistivity in inhomogeneous materials.

DOI: 10.1103/PhysRevB.84.064408 PACS number(s): 72.15.Eb, 72.15.Gd, 74.70.Dd

I. INTRODUCTION

The recent reports of a positive, extraordinarily high, linear magnetoresistivity (LMR) in nonmagnetic semimetals and semiconductors have attracted much attentions.[1–17] Extensive efforts were directed toward the identification of the involved mechanism(s) as well as toward material optimization for eventual technological applications, such as high-density data storage or magnetic sensors and actuators. LMR was observed over wide ranges of temperatures ($\sim$mK $\leqslant T \leqslant$ 400 K) and magnetic fields (few Oe $\leqslant H \leqslant$ 600 kOe) and in a variety of materials, such as elemental metals,[2–4] intermetallic compounds,[5–7] $Ag_{2+\delta}X$ (X = Se, Te),[8–11] InSb,[12] Si,[13] graphene,[14] graphite,[15] GaAs-MnAs,[16] and $BaFe_2As_2$.[17]

Classically, a field-dependent, normalized magnetoresistivity $\Delta\rho_T(H)/\rho_T(0) = [\rho_T(H) - \rho_T(0)]/\rho_T(0)$ is quadratic in H for $\mu_c H/c < 1$ and saturates for $\mu_c H/c > 1$ (carrier mobility $\mu_c = e\tau/m^*$; symbols have their usual meaning). Various scenarios,[1] with some classical and others quantum mechanical, were proposed for the interpretation of the deviation of LMR from the classical prediction.

The so-called Kapitza's LMR is expected in metals, such as Bi, with an open Fermi surface and a mean-free path which is longer than the electronic Larmor radius.[2–4] Another scenario discusses the inhomogeneous conducting media, such as InSb semiconductor above 200 K: here disorder causes an intermixing of the off-diagonal components of the magnetoresistive (MR) tensor and, as such, the associated LMR is due to the distribution in μ_c, rather than μ_c itself.[12]

Abrikosov[1] identified three classes of materials wherein quantum LMR can be manifested. First are those homogenous materials at very low T and strong H and with a low concentration of charge carriers (n_c) and a small m^*, such that only the lowest Landau level is populated. Its strength is given by $N_d H/(\pi n_c^2 ec)$, where N_d is the concentration of the defect centers. Second are those highly inhomogeneous materials, e.g., $Ag_{2+\delta}X$ (X = Se, Te),[8–11] wherein metallic inclusions (with higher n_c) are dispersed within a matrix having a smaller n_c, a linear dispersion relation, and a vanishing energy gap. Third are those layered structures such as $LaSb_2$,[5,6] which—due to a particular configuration of their electronic structure—exhibit a large Fermi surface (with a classical MR contribution) and, in addition, tiny pockets with a small effective mass (thus providing a quantum LMR contribution). In this case, depending on T, H, and the material properties, LMR may dominate the magnetoresistive feature.

In this work, we report on the observation of a relatively strong LMR effect in the homologous $A_nM_{3n-1}B_{2n}$ series (A = Ca, Sr; M = Rh, Ir; n = 1, 3). Because the evolution of LMR depends on material parameters such as n_c, μ_c, and anisotropy, the investigation of MR in different $A_nM_{3n-1}B_{2n}$ members (each with its distinct materials properties) would be helpful in identifying the essential parameters behind the surge of LMR in this series. In fact, the following three reasons highlight our interest in studying the functional dependence of LMR in these intermetallics. First, their structure consists of a combination of alternatively stacked AM_2B_2 and AM_3B_2 sheets (see Fig. 1).[18] As such, a variation in n (e.g., $1 \leftrightarrow 3$) entails a variation in the number of involved layers and, as a consequence, a variation in the electronic properties. Second, a variation of A (Ca $\leftrightarrow$ Sr) or M (Rh $\leftrightarrow$ Ir) entails also a possible variation in n_c, μ_c, or chemical pressure. Third, because both $Sr_3Rh_8B_6$ and $Ca_3Rh_8B_6$ are superconductors while AM_2B_2 are normal,[19] and, furthermore, because all members show a LMR effect, it is interesting to investigate the correlation, if there is any, between the electronic ground state (whether superconducting or normal) and their LMR properties.

II. EXPERIMENT

Six compounds, AM_2B_2 and $A_3Rh_8B_6$ (A = Ca, Sr; M = Rh, Ir), were synthesized using the standard solid-state reaction of pure elements in BN or Ta crucibles (in contrast to the $A_nRh_{3n-1}B_{2n}$ case, there is no homologous Ir-based $n = 3$ series). Their single phase character was verified by extensive structural and elemental analyses (see Ref. 19 for information on the synthesis, structural, and elemental analyses).

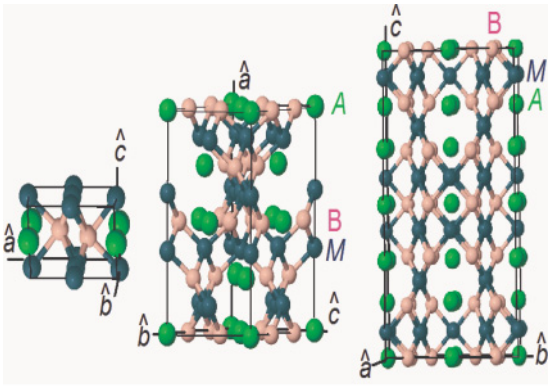

FIG. 1. (Color online) The unit cells, not to scale, of (a) AM_3B_2 ($P6/mmm$),[20] (b) AM_2B_2 ($Fdd2$), and (c) $A_3M_8B_6$ ($Fmmm$) (A = Ca, Sr; M = Rh, Ir). The structure of $A_3M_8B_6$ can be visualized as an alternating stacking of the (a) AM_3B_2 and (b) AM_2B_2 sheets.[18] The stacking direction for AM_3B_2, AM_2B_2, and A_3M_8 B_6 is along the c, a, and c axis, respectively.

$\rho(T,H)$ curves of polycrystalline, parallelepiped-shaped samples were measured by a conventional, home-made, in-line, four-point magnetoresistometer. The geometry of the sample as well as the separation between the contacts were chosen in such a way as to reduce the contribution of the so-called geometrical magnetoresistivity, which is a purely geometrical effect associated with the response to the changing direction of the current carriers in a magnetic field.[21] The longitudinal geometry ($I \| H$) was adopted in most cases so as to avoid such a geometrical effect and also to detect any possible Shubnikov-de Haas oscillations.[22] As a check, $\rho(T,H)$ of $Ca_3Rh_8B_6$ was measured also along the transversal geometry ($I \perp H$): as usual,[6,12] the transverse $\Delta\rho_T(H)/\rho_T(0)$ is much higher than the longitudinal one. The ohmic character was verified within the $1 \leqslant I \leqslant 100$ mA range for various samples; measurements reported here were taken with 10 mA. Various isofield and isothermal scans were carried out covering $1.8 \leqslant T \leqslant 300$ K and $0 \leqslant T \leqslant 50$ kOe. The residual resistivity ratio, $RRR = \rho(300\text{ K})/\rho(1.8\text{ K})$, was found to be ~6–32. $\rho(T, H = 0)$ was considered to be a sum of a residual contribution ρ_{00} and a Bloch-Grüneisen (BG) expression,[23]

$$\rho_0(T) - \rho_{00} = 16\pi^2\omega_D\frac{\lambda}{\omega_p^2}\left(\frac{2T}{\theta_D}\right)^5\int_0^{\frac{\theta_D}{2T}}\frac{x^5}{\sinh(x)^2}dx, \qquad (1)$$

where λ is the electron-phonon coupling, ω_p is the Drude plasma frequency, and ω_D is the Debye phonon frequency. Below, only θ_D and λ/ω_p^2 are treated as free parameters.

Low-T $\rho_T(H)$ isotherms exhibit a strong linear-in-H feature for $H > H_{cr} \approx 10$ kOe (H_{cr} is the crossover field above which the LMR character dominates). Thus for $H > H_{cr}$ and $T < 100$ K,

$$\Delta\rho_T(H)/\rho_T(0) = a_0 + a_T H, \qquad (2)$$

where $a_T = (\frac{1}{\rho_{0T}}\frac{\partial\rho}{\partial H})_T$ depends on T and the material properties. Plots of $\Delta\rho_T(H)/\rho_T(0)$ isotherms against H/ρ_o indicate that the Kohler rule is not satisfied. The thermal evolution of $\Delta\rho_{50\,kOe}(T)/\rho_0(T) = [\rho_{50\,kOe}(T) - \rho_0(T)]/\rho_0(T)$ was found to follow the empirical relation,

$$\Delta\rho_{50\,kOe}(T)/\rho_0(T) = b_H \tanh(c_H/T)/[d_H T^2 + 1], \qquad (3)$$

where the phonon contribution was assumed to be H independent,[24] and b_H, c_H, and d_H are sample-dependent parameters that will be used below only for comparative purposes. Above 100 K, this expression (and its LMR character) was found to be extremely small, suggesting an energy scale of ~9 meV. Finally, for $T \to \infty$, $\Delta\rho_{50kOe}(T)/\rho_0(T) \to T^{-3}$; on the other hand, if both Eqs. (2) and (3) hold as $T \to 0$ K, then $b_H \to a_0 + a_T H$. This establishes a link to available theoretical models.

III. RESULTS

A. $Ca_nRh_{3n-1}B_{2n}$ (n = 1,3) and $CaIr_2B_2$

Figure 2(a) emphasizes the metallic character of the zero-field $\rho_0(T)$ curve of $CaRh_2B_2$; it follows the BG description [see Eq. (1) and Table I] emphasizing the dominant strength of the phonon-electron interaction. In addition, Fig. 2 (in particular, the insets) manifests a relatively strong $\Delta\rho/\rho_o$, in which $\Delta\rho_{50kOe}(T)/\rho_0(T)$ is relatively strong (>100%) at low T, but decreases sharply with temperature (below 4% for temperatures above 100 K) following approximately Eq. (3) [see inset of Figs. 2(a), 3(a), and Table I].

Similar conclusions were drawn from the analysis of various $\rho_T(H)$ isotherms, where all $\Delta\rho_T(H)/\rho_T(0)$ isotherms of Fig. 2(b) manifest a positive MR with a positive curvature (concave upwards) and a predominant high-H LMR character. Fitting $\Delta\rho_T(H > 10\,kOe)/\rho_T(0)$ to Eq. (2) gave the parameter

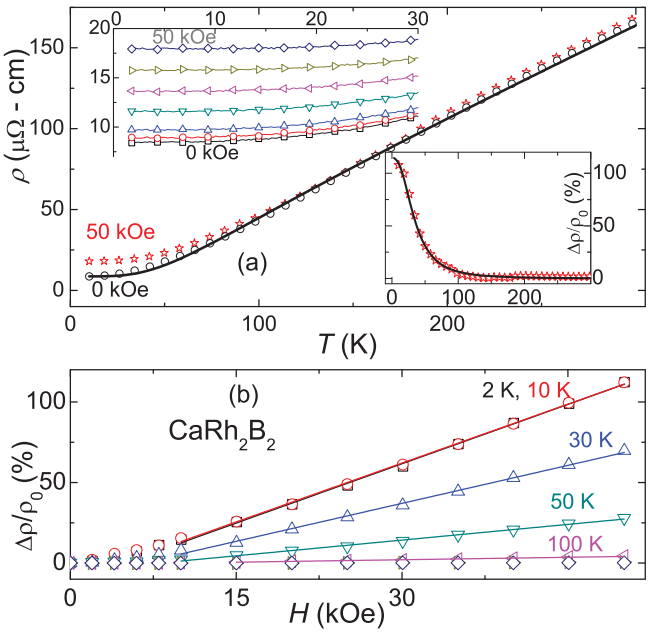

FIG. 2. (Color online) $\rho(H,T)$ curves of $CaRh_2B_2$. (a) Isofield $\rho_H(T)$ curves at $H = 0$ and 50 kOe [solid line, $H = 0$, is a fit to Eq. (1)]. Inset (upper left): Isofield $\rho_H(T)$ curves at H = 0, 5, 10, 20, 30, 40, 50 kOe. Inset (lower right): Thermal evolution of $\Delta\rho_{50\,kOe}(T)/\rho_0(T)$ [solid line represents Eq. (3)]. (b) $\Delta\rho_T(H)/\rho_T(0)$ isotherms [solid lines are fits to Eq. (2)].

TABLE I. The parameters b_H, c_H, and d_H were obtained from fitting longitudinal $\Delta\rho_{50\,kOe}(T)/\rho_0(T)$ to Eq. (3) [bracketed values represent transverse geometry]. θ and λ/ω^2 are from the BG fit [Eq. (1)]. RRR represents $\rho(300\,K)/\rho$ (1.8 K). The high RRR of the $n = 3$ members is related to the onset of partial superconductivity. $\rho_{50kOe}(T)$ increases with H, θ (lattice hardening), and ρ_0 (residual resistivity).

A_n	parameter	$n = 1$		$n = 3$
		Rh	Ir	Rh
$Ca_nRh_{3n-1}B_{2n}$				
	RRR	19.3	32.2	13.5
	$\theta \pm 10$ K	280	380	200[200]
	$\lambda\omega_D/\omega_p^2$ ($\times 10^{-4}\Omega$ cm)	19.2	18.4	5.2[5.1]
	b_H	115	80	47[85]
	c_H	35	30	35[33]
	$d_H(\times 10^{-4}$ K$^{-2})$	5	4	3.4[3.4]
$Sr_nRh_{3n-1}B_{2n}$				
	RRR	13.9	12.3	6.0
	$\theta \pm 10$ K	300	250	280
	$\lambda\omega_D/\omega_p^2$ ($\times 10^{-4}\Omega$ cm)	5.7	6.1	8.4
	b_H	13	22	3.5
	c_H (K)	100	57	90
	$d_H(\times 10^{-4}$ K$^{-2})$	1.75	4	0.7

plotted in Fig. 3(b) which, once more, emphasizes the strong T dependence of $\Delta\rho_T(H)/\rho_T(0)$.

In contrast to $CaRh_2B_2$, low-T $\rho(H,T)$ of $Ca_3Rh_8B_6$ (Fig. 4) show a superconducting state[19] below $T_c \approx 4$ K and, surprisingly, the resistivity within the superconducting phase does not completely vanish, indicating an absence of percolation. Above T_c, the normal metallic state follows a BG description [Fig. 4(a) and Table I]; however, for temperatures above 230 K, there is a weak deviation away from Eq. (1). A sizable $\Delta\rho_T(H)/\rho_T(0)$ is evident in most curves of Fig. 4; in

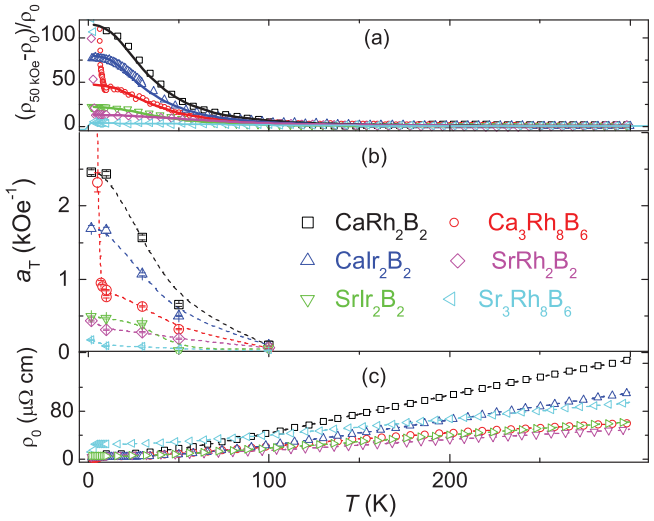

FIG. 3. (Color online) Thermal evolution of (a) longitudinal $\Delta\rho_{50kOe}(T)/\rho_0(T)$ [solid lines are fits to Eq. (3)], (b) a_T [based on fit to Eq. (2)], and (c) the measured zero field $\rho_0(T)$. For the three panels, the anomalous features of $A_3Rh_8B_6$ (A = Ca, Sr) at the lowest temperatures are related to the onset of superconductivity.[19]

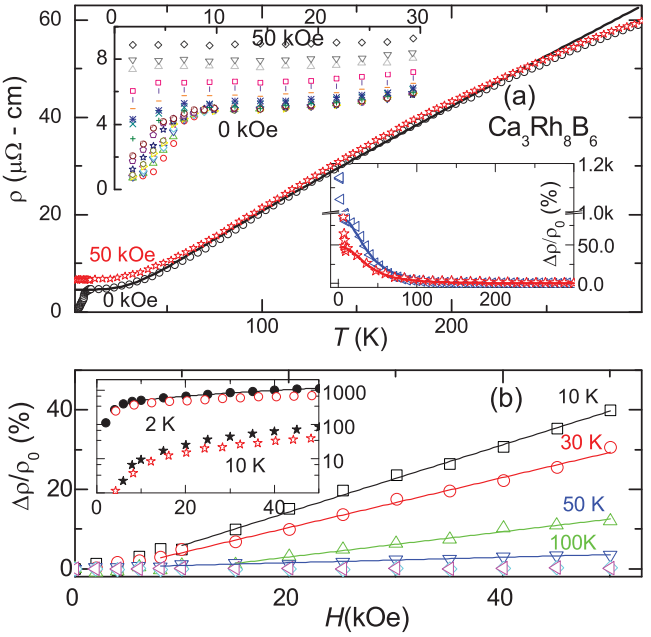

FIG. 4. (Color online) $\rho(H,T)$ curves of $Ca_3Rh_8B_6$. (a) $\rho_H(T)$ curves at $H = 0$ and 50 kOe [solid line, $H = 0$, is a fit to Eq. (1)]. Inset (upper left): thermal evolution of isofield $\rho_H(T)$ curves at $H = 0, \ldots, 50$ kOe. Inset (lower right): thermal evolution of $\Delta\rho_{50kOe}(T)/\rho_0(T)$ curves [triangles are transversal; stars are longitudinal; solid lines are fits to Eq. (3)]. (b) Longitudinal $\Delta\rho_T(H)/\rho_0(0)$ isotherms [solid lines are fits to Eq. (2)]. Inset: A semilogarithmic plot of the $\Delta\rho_T(H)/\rho_T(0)$ isotherms at 2 and 10 K; filled (open) symbols represent transversal (longitudinal) arrangement.

particular, Fig. 4(b) shows that $\rho_{T<T_c}(H > H_{c2})$ manifests a negative curvature, while $\rho_{T>T_c}(H)$ manifests a positive and almost linear evolution. Fitting these curves to Eq. (2) yielded a_T, the thermal evolution of which is plotted in Fig. 4.

The normalized $\Delta\rho_{1.8K}(H)/\rho_{1.8K}(0)$ reaches, at 50 kOe, an impressive value of 1200% [see inset of Fig. 4(b)]. This is attributed to the presence of the superconducting state [a much higher value would be attained if $\rho_T(0)$ is decreased further].

Figure 5 of $CaIr_2B_2$ reflects the same features that were observed in $CaRh_2B_2$: a metallic $\rho_T(0)$ with a BG character (Table I), a predominant LMR feature, and a relatively strong $\Delta\rho_{50kOe}(T)/\rho_0(T)$ effect at low T, but decays rapidly at higher T, dropping to below 3% above 100 K. The a_T parameter [the fit of $\rho_T(H)$ to Eq. (2), Fig. 5(b)] is shown in Fig. 3.

B. $Sr_nRh_{3n-1}B_{2n}$(n = 1,3) and $SrIr_2B_2$

$\rho(H,T)$ curves of $SrRh_2B_2$ (Fig. 6) manifest magnetoresistive features that are very similar to those found in $CaRh_2B_2$, except that the strength of the effect is smaller and there is a weak superconducting secondary phase (namely, $Sr_3Rh_8B_6$), which is believed to be behind the drop in the magnetoresistivity of $SrRh_2B_2$ below that of $SrIr_2B_2$ (compare Figs. 3 and 6). On the other hand, Fig. 7 shows that $Sr_3Rh_8B_6$ superconducts below $T_c \approx 3.5$ K, exhibits a BG-type resistivity above T_c, and has MR features that are very similar to, but almost two orders of magnitude weaker than, those of $Ca_3Rh_8B_6$.

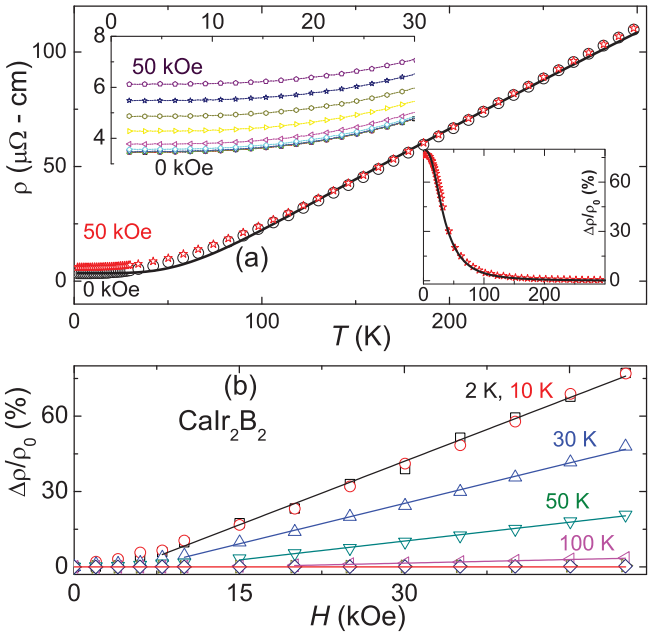

FIG. 5. (Color online) $\rho(H,T)$ curves of $CaIr_2B_2$. (a) Isofield $\rho_H(T)$ curves at $H = 0$ and 50 kOe [solid line, $H = 0$, is a fit to Eq. (1)]. Inset (upper left): thermal evolution of isofield $\rho_H(T)$ curves at $H = 0, \ldots, 50$ kOe. Inset (lower right): thermal evolution of $\Delta\rho_{50kOe}(T)/\rho_0(T)$ curve [solid line is a fit to Eq. (3)]. (b) The $\Delta\rho_T(H)/\rho_T(0)$ isotherms [solid lines are fits to Eq. (2)].

Similar to the cases found in CaM_2B_2 isomorphs, $\rho(H,T)$ of $SrIr_2B_2$ (Fig. 8) show all the features that we mentioned above: the metallic resistivity obeying a BG description, the

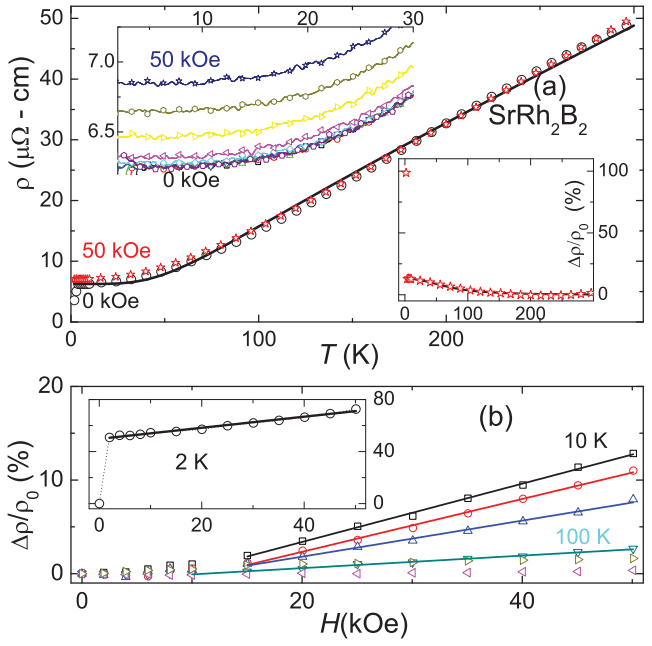

FIG. 6. (Color online) $\rho(H,T)$ curves of $SrRh_2B_2$. (a) Isofield $\rho_H(T)$ curves at $H = 0$ and 50 kOe [solid line, $H = 0$, is a fit to Eq. (1)]. Inset (upper left): thermal evolution of isofield $\rho_H(T)$ curves at $H = 0, \ldots, 50$ kOe. Inset (lower right): $\Delta\rho_{50\,kOe}(T)/\rho_0(T)$ curve [solid line is a fit to Eq. (3)]. (b) $\Delta\rho_T(H)/\rho_T(0)$ isotherms [solid lines are fits to Eq. (2)].

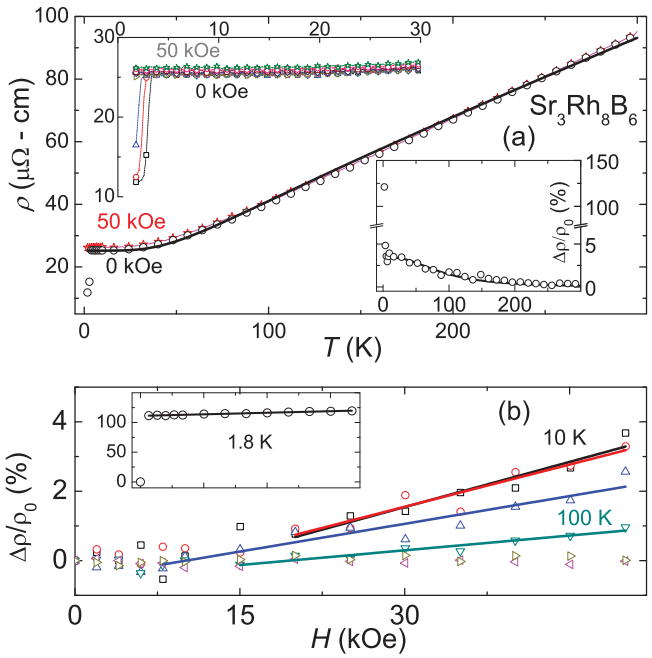

FIG. 7. (Color online) $\rho(H,T)$ curves of $Sr_3Rh_8B_6$. (a) Isofield $\rho_H(T)$ curves at $H = 0$ and 50 kOe [solid line, $H = 0$, is a fit to Eq. (1)]. Inset (upper left): Thermal evolution of isofield $\rho_H(T)$ curves at $H = 0, \ldots, 50$ kOe. Inset (lower right): $\Delta\rho_{50kOe}(T)/\rho_0(T)$ curve [solid line is a fit to Eq. (3)]. (b) $\Delta\rho_T(H)/\rho_T(0)$ isotherms [solid lines are fits to Eq. (2)]. Inset: An expansion of the $\Delta\rho_{1.8K}(H)/\rho_{1.8K}(0)$ isotherm.

predominantly LMR character, and the strong T dependence of $\Delta\rho_{50kOe}(T)/\rho_0(T)$ up to 100 K. From a fit of $\Delta\rho_T(H)/\rho_T(0)$ to Eq. (2), we obtained a_T (given in Fig. 3).

IV. DISCUSSION AND CONCLUSIONS

Our experiments indicated that $\Delta\rho_T(H)/\rho_T(0)$ of $A_nM_{3n-1}B_{2n}$ is positive, nonsaturating, and dominantly linear above ~10 kOe, and that a relatively strong $\Delta\rho_T(H)/\rho_T(0)$ was observed in both superconducting and normal members, which decreases sharply with temperature and whenever n is increased, Rh is replaced by Ir, or Ca is replaced by Sr. These features, as well as other magnetoresistive properties of the studied members, were compared in Fig. 3 and Table I; evidently the Ca-based isomorphs exhibit a higher RRR, a higher λ/ω_p^2, and a higher $\Delta\rho_T(H)/\rho_T(0)$.

It is recalled that a reduction in the LMR is usually related to an increase in n_c, μ_c, or a decrease in N_d (for a quantum LMR, a smearing of the Landau levels).[12] In turn, the variation in any of n_c, μ_c, or N_d (ρ_0) can be straightforwardly associated with a related variation in T, H, or the material properties. Along this line of arguments, we discuss the above-mentioned MR features of $A_nM_{3n-1}B_{2n}$ series.

First, the drop in $\Delta\rho/\rho_0$ with increasing n is attributed to an increase in n_c. Because the structure of $A_3M_8B_6$, in contrast to AM_2B_2, includes additional, sandwiched AM_3B_2 layers (Fig. 1), it is inferred that the introduction of AM_3B_2 enhances n_c.[25] In fact, rewriting the $n = 3$ member as $A_1M_{8/3}B_2$ already suggests that this enhancement is due to a contribution from the $4d^85s^1$ subbands of the extra Rh. Such a higher n_c is consistent

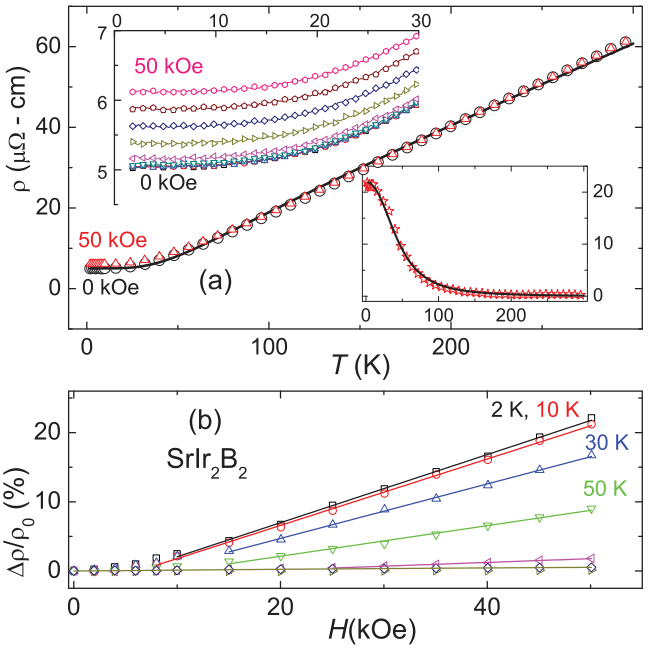

FIG. 8. (Color online) $\rho(H,T)$ curves of $SrIr_2B_2$. (a) Isofield $\rho_H(T)$ curves at $H = 0$ and 50 kOe [solid line, $H = 0$, is a fit to Eq. (1)]. Inset (upper left): Thermal evolution of isofield $\rho_H(T)$ curves at $H = 0, \ldots, 50$ kOe. Inset (lower right): $\Delta\rho_{50\,kOe}(T)/\rho_0(T)$ curve [solid line is a fit to Eq. (3)]. (b) $\Delta\rho_T(H)/\rho_T(0)$ isotherms [solid lines are fits to Eq. (2)].

with the surge of superconductivity in the $n = 3$ members.[19] Second, the fact that the resistivity within the superconducting state of $A_3Rh_8B_6$ does not vanish is an indication that these $n = 3$ samples contain superconducting regions dispersed within a nonsuperconducting matrix. This feature excludes the applicability of the classical LMR models; rather it supports the Abrikosov LMR scenario for inhomogeneous media.[1]

By generalizing this inhomogeneous configuration to the $n = 1$ members[26] and assuming the variation in the LMR effect to be related to a corresponding variation in either n_c or carrier dynamics (influenced by pressure, charge doping, T, or H), the above-mentioned experimental results can be satisfactorily explained. As an example, the fact that $\Delta\rho/\rho_0$ of Sr-based compounds are lower than their Ca-based isomorphs is attributed to a negative chemical pressure, which is induced by the substitution of isovalent, relatively large-sized Sr^{+2} into the Ca^{+2} site. Similarly, the reduction of $\Delta\rho/\rho_0$ caused by the replacement of Rh by Ir ($5d^75s^2$) is attributed to an increase in n_c that overwhelms the influence of an increased antisymmetric spin-orbit interaction. It is recalled that the space group of AM_2B_2 is $Fdd2$ (having no inversion symmetry operator),[19] while the space group of $A_3M_8B_6$ is $Fmmm$ (with an inversion symmetry operator). Accordingly, the antisymmetric spin-orbit interaction in the former series would exercise a considerable influence (via a spin splitting of the quasiparticle states) on the electronic properties.[27] According to Abrikosov,[1] a linear spectrum may arise due to an absence of a symmetry inversion centre. Because a linear spectrum implies a smaller effective mass, the absence of a symmetry inversion would enhance the quantum LMR of the $n = 1$ members. Finally, the thermal rate of decrease of $\Delta\rho_T(H)/\rho_T(0)$ in $A_nM_{3n-1}B_{2n}$ is much faster than that of, say, $Ag_{2+\delta}X$ (X = Se, Te) (Ref. 8) but similar to that of $LaSb_2$ (Ref. 6) as n_c hardly varies below 300 K; this thermal decrease is attributed to the phonon-driven decrease in μ_c and a smearing of the Landau levels.[16]

In summary, a positive, nonsaturating, and dominantly linear MR was observed in the $A_nM_{3n-1}B_{2n}$ series (A = Ca, Sr; M = Rh, Ir, $n = 1$, 3). This effect was found to decrease whenever n is increased, Ca is replaced by Sr, Rh is replaced by Ir, or the temperature is raised. Comparative MR studies among the different members suggest that LMR can be described by the Abrikosov model for inhomogeneous media.

ACKNOWLEDGMENTS

We acknowledge partial financial support from the Japan Society for the Promotion of Science and the Brazilian agencies CNPq and Faperj.

*takeya.hiroyuki@nims.go.jp
†massalam@if.ufrj.br

[1] A. A. Abrikosov, J. Phys. A **36**, 9119 (2003).
[2] P. L. Kapitza, Proc. R. Soc. A **123**, 292 (1929).
[3] K. Liu, C. L. Chien, and P. C. Searson, Phys. Rev. B **58**, R14681 (1998).
[4] F. Y. Yang, K. Liu, D. H. Reich, P. C. Searson, and C. I. Chien, Science **284**, 1335 (1999).
[5] S. L. Bud'ko, P. C. Canfield, C. H. Mielke, and A. H. Lacerda, Phys. Rev. B **57**, 13624 (1998).
[6] D. P. Young, R. G. Goodrich, J. F. DiTusa, S. Guo, P. W. Adams, J. Y. Chan, and D. Hall, Appl. Phys. Lett. **82**, 3713 (2003).
[7] M. Andersson, M. Feuerbacher, and Ö. Rapp, Phys. Rev. B **78**, 024201 (2008).
[8] R. Xu, A. Husmann, T. F. Rosenbaum, M.-L. Saboungi, J. E. Enderby, and P. B. Littlewood, Nature (London) **390**, 57 (1997).
[9] A. Husmann, J. B. Betts, G. S. Boebinger, A. Migliori, T. F. Rosenbaum, and M. L. Saboungi, Nature (London) **417**, 421 (2002).
[10] M. Lee, T. F. Rosenbaum, M.-L. Saboungi, and H. S. Schnyders, Phys. Rev. Lett. **88**, 066602 (2002).
[11] M. von Kreutzbruck, G. Lembke, B. Mogwitz, C. Korte, and J. Janek, Phys. Rev. B **79**, 035204 (2009).
[12] J. Hu and T. F. Rosenbaum, Nature Mater. **7**, 697 (2008).
[13] M. P. Delmo, S. Yamamoto, S. Kasai, T. Ono, and K. Kobayashi, Nature (London) **457**, 1112 (2009).
[14] A. L. Friedman *et al.*, Nano Lett. **10**, 3962 (2010).
[15] S. V. Morozov, K. S. Novoselov, F. Schedin, D. Jiang, A. A. Firsov, and A. K. Geim, Phys. Rev. B **72**, 201401(R) (2005).
[16] H. G. Johnson, S. P. Bennett, R. Barua, L. H. Lewis, and D. Heiman, Phys. Rev. B **82**, 085202 (2010).
[17] N. Tajima, S. Sugawara, R. Kato, Y. Nishio, and K. Kajita, Phys. Rev. Lett. **106**, 217004 (2011).

[18] W. Jung, J. Less-Common Met. **97**, 253 (1984).
[19] H. Takeya and M. ElMassalami (unpublished).
[20] *Inorganic Crystal Structure Database* [http://icsd.fiz-karlsruhe.de/]
[21] D. Schroder, *Semiconductor Material and Device Characterization* (Wiley, New York, 2006).
[22] Due to the limited temperature range and disorder in the samples, we were unsuccessful in observing Shubnikov-de Haas oscillations.
[23] P. B. Allen, in *Quantum Theory of Real Materials*, edited by J. R. Chelikowsky and S. G. Louie (Kluwer, Boston, 1996), p. 319.
[24] LMR is stronger at temperatures where phonon density is extremely small.
[25] The magnetoresistivity of AM_3B_2 is expected to be very small.
[26] $A_nRh_{3n-1}B_{2n}$ (A = Ca, Sr), being incongruent phases, were precipitated via peritectic reactions from an A-rich composition. Therefore some excess A melts may form around the desired phase or be segregated elsewhere.
[27] V. P. Mineev and M. Sigrist, e-print arXiv:0904.2962v2.